

Binary Apollonian networks

Eduardo M. K. Souza¹ and Guilherme M. A. Almeida²

¹*Departamento de Física, Universidade Federal de Sergipe, 49100-000 São Cristóvão, Sergipe, Brazil*

²*Instituto de Física, Universidade Federal de Alagoas, 57072-900 Maceió, Alagoas, Brazil*



(Received 30 June 2022; accepted 31 January 2023; published 10 February 2023)

There is a well-known relationship between the binary Pascal's triangle and the Sierpinski triangle, in which the latter is obtained from the former by successive modulo 2 additions starting from a corner. Inspired by that, we define a binary Apollonian network and obtain two structures featuring a kind of dendritic growth. They are found to inherit the small-world and scale-free properties from the original network but display no clustering. Other key network properties are explored as well. Our results reveal that the structure contained in the Apollonian network may be employed to model an even wider class of real-world systems.

DOI: [10.1103/PhysRevE.107.024305](https://doi.org/10.1103/PhysRevE.107.024305)

I. INTRODUCTION

Network theory has brought significant advances to the field of complex systems, being applied to the spread of diseases and information, author collaboration networks, engineering, condensed-matter physics, transport, and much more [1,2]. While many types of networks are used to model the dynamics of those and other classes of systems, they often share a lot in common. To bypass complexity and reach for perspective, it is thus valuable to explore their universal properties. For instance, real-world networks are neither fully random nor fully regular but fit somewhere in between. As such, many of them display features belonging to the class of small-world networks [3]. These are graphs where it is often possible to go from one node to another by taking a small number of steps. Formally, it means the characteristic path length grows logarithmically with the number of nodes, while retaining a clustering coefficient well above that of a random graph.

A paradigmatic example of a graph displaying the small-world property is the Apollonian network (AN) [4] (see Fig. 2), named after Apollonius' circle-packing ideas. This class of networks is also scale free (the degree distribution follows a power law) and can be embedded in the Euclidean plane, which is quite relevant to condensed-matter physics. ANs have since been used in the context of strongly correlated electron systems [5], Bose-Einstein condensation [6], localization [7], quantum dynamics [8,9], and other fields [10–13]. In particular, their topology yields ubiquitous transport properties as the spectrum is made up of discrete, localized modes as well as extended modes, with a high level of degeneracy due to the node degree distribution and $2\pi/3$ rotational symmetry [9].

The primary goal of investigating complex networks is to provide insights into the behavior of real-world systems, either natural or manufactured. In order to do that, one should be able to identify them accurately, something not always considered. On the other hand, seemingly distinct structures may display very similar behavior. From a more fundamental level, we may ask ourselves what main ingredients are responsible

for that. Following this direction, in this work we set out to take a better look into the building blocks of the AN. We derive subnetworks inspired by the well known relationship between the binary Pascal's triangle and the Sierpinski triangle. The latter is a fascinating fractal structure that emerges from various systems in nature and is connected to many areas of mathematics. It can be obtained, for example, from the Pascal's triangle by assigning a binary number, 0 or 1, to each element based on its even or odd parity, respectively. It is easy to see that the larger the triangle is (see Fig. 1), the more its binary structure converges to the Sierpinski fractal. It can also be generated from scratch by performing successive modulo 2 additions in the Pascal's triangle.

Based on such a construction we define a binary AN where to each node is assigned a bit that is the result of the modulo 2 addition of the three nodes (from the previous generation) surrounding it. Two subnetworks arise from such a procedure and we will address them in detail by evaluating standard measures such as the degree distribution, clustering coefficient, mean distance, and spectrum of the adjacency matrix.

II. APOLLONIAN SUBNETWORKS

The regular AN is built starting out with a triangle (zeroth generation, $n = 0$) as depicted in Fig. 2. In the following generation ($n = 1$), a new node is added within it and the edges now form three triangles. Subsequent generations are obtained by repeating this process for each triangle to render a self-similar network. To build a binary version of the AN we assign a bit to each node. Consider the blue circles (red squares) to represent bit 0 (1) in Fig. 2. Subsequent nodes are defined according to the modulo 2 addition of the bits that form their respective triangle. From generation $n = 0$ we note that out of the many possibilities to set the three initial bits, they will either deliver the standard network or amount to the construction seen in Fig. 2. This summarizes the output whenever one bit is different from the other two.

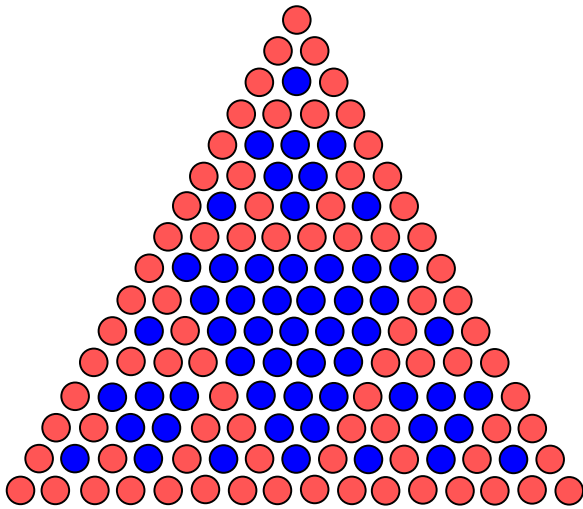


FIG. 1. A structure resembling the Sierpinski fractal triangle can be obtained from the famous Pascal's triangle by carrying out successive modulo 2 additions downward. Red (light) circles stand for bit 1 and blue (dark) circles represent bit 0.

We have obtained two groups of nodes in the AN. If we now split them up keeping only their own links (edges connecting different bits are destroyed), a couple of subnetworks emerge. Figures 3 and 4 show each one of them in detail from a clearer perspective starting from $n = 2$. For convenience, we will refer to those as 0-AsN and 1-AsN, respectively, from now on. Both structures can be easily treated by their own growth rules without looking back at the original AN. For each new generation, every node is joined by a number of new others equal to the number of edges it had in the previous

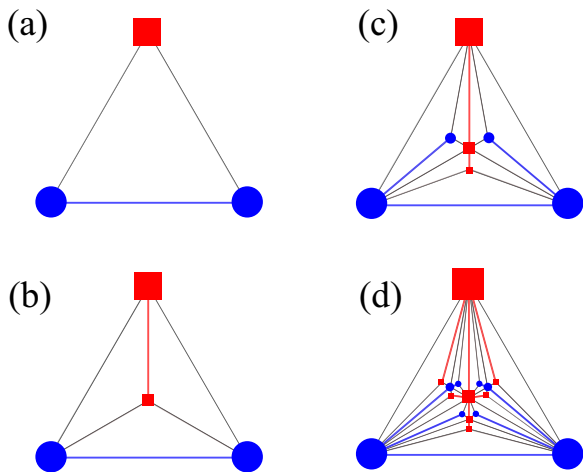


FIG. 2. Apollonian network from the (a) zeroth generation ($n = 0$) through the (d) third ($n = 3$). The total number of sites is $N_n = (3^n + 5)/2$, and the number of edges is $B_n = 3N_n - 6$. To build its binary version we assign a bit to each one of the nodes. Here, blue circles (red squares) represent bit 0 (1). Each node belonging to subsequent generations is set according to the modulo 2 sum of the three nodes surrounding it that form a triangle. The Apollonian subnetworks are defined by detaching both groups of bits keeping their own bonds.

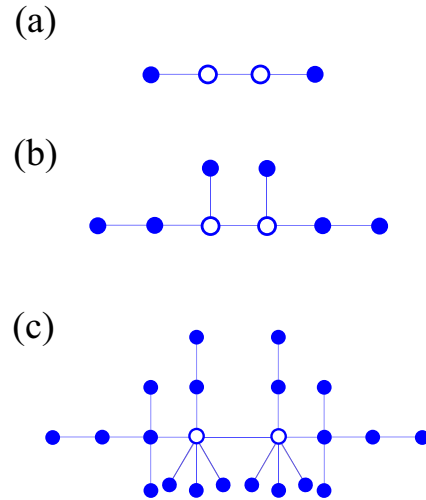


FIG. 3. Apollonian subnetwork made up by the bit-0 nodes (0-AsN) for generations (a) $n = 2$ (b) $n = 3$, and (c) $n = 4$. Empty circles represent both nodes located at the bottom corners of the original network.

generation, with a few exceptions. In the 0-AsN, the nodes located at the bottom corners of the original network (see Fig. 2), represented by the empty circles in Fig. 3, acquire one bond less when going from an even to an odd generation. In the 1-AsN, the node located at the top corner of the AN, tagged as the empty square in Fig. 4, gets an extra neighbor when going from an even to an odd generation and one less otherwise. Aside from these exceptions, both subnetworks follow construction rules commonly set for general treelike graphs [14]. Ours are particularly homogeneously weighted and are built such that a new node is attached to each edge end

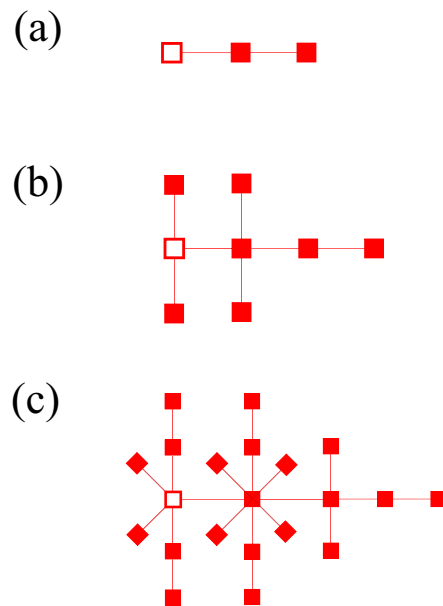


FIG. 4. Apollonian subnetwork made up by the bit-1 nodes (1-AsN) for generations (a) $n = 2$ (b) $n = 3$, and (c) $n = 4$. An empty square represents the node located at the top corner of the original network.

from the previous generation [15]. Also note that the growth process of such networks resembles those seen in deposition of materials that develop a dendritic pattern [16].

The total number of sites in the standard, n th generation AN is $N_n = (3^n + 5)/2$ and the number of edges $B_n = 3N_n - 6$ [4]. For the 0-AsN and 1-AsN, it is straightforward to obtain that $N_n = [3^n + (-1)^n + 6]/4$ and $N_n = [3^n - (-1)^n + 4]/4$, respectively. The number of edges is $B_n = N_n - 1$ for both cases.

III. PROPERTIES

We now move on to evaluate some fundamental properties of both subnetworks and compare them with the original AN [4]. Let us start with the degree of a node, that is the number of edges connected to it, $k_i = \sum_j A_{i,j}$, where $A_{i,j}$ are the entries of the corresponding adjacency matrix \mathbf{A} ($A_{i,j} = 1$ if there is an edge between nodes i and j , with $A_{i,j} = 0$ otherwise). Here any node can be fully assigned by the generation ν that gave rise to it and thus $k = k(\nu, n)$. Also, let $m = m(k, n)$ be the number of nodes with degree k at a given generation n . In the AN the three nodes arranged at the corners (present since $\nu = 0$) have degree $k = 2^n + 1$. A set of $m = 3^{n-1}$ nodes is introduced at every new generation $n \geq 1$ with degree $k = 3$. Therefore $m = 3^{v-1}$ nodes that surged in generation $\nu \leq n$ acquire $k = 3 \times 2^{n-\nu}$ edges. Note that the hub corresponds to $\nu = 1$. Now, the 0-AsN has two hubs—depicted as empty circles in Fig. 3—satisfying $k = [2^{n+1} + (-1)^n + 3]/6$ ($n \geq 0$). Every other node that takes place at $\nu \geq 2$ is part of a group of $m = [3^{v-1} + (-1)^v]/2$ nodes with the same hierarchy featuring $k = 2^{n-\nu}$ edges. The 1-AsN features a single hub instead (located at the right of the empty square in Fig. 3), with $k = 2^{n-1}$, whereas the node that stands for the top corner of the original AN has $[2^n + (-1)^{n-1}]/3$. For the remaining network, one gets $m = [3^{v-1} + (-1)^{v-1}]/2$ nodes with degree $k = 2^{n-\nu}$ ($\nu \geq 2$).

Using the information above we can show the subnetworks are scale free, just like the AN. This property can be confirmed through the cumulative distribution

$$P(k) = \sum_{k' \geq k} \frac{m(k', n)}{N_n}, \quad (1)$$

which is displayed in Fig. 5. For $n \gg 1$, we get the typical asymptotic power-law decay $P(k) \propto k^{-\gamma}$. The exponent can be evaluated directly from the expressions for $m(k, n)$, N_n , resulting in $\gamma = \ln 3 / \ln 2 = 1.585$ for all the networks. Note that this value is exactly the Hausdorff dimension of the Sierpinski triangle [17], which is not a mere coincidence, since it has the same combinatorial structure as the Apollonian gasket.

Let us now check their connectance, defined by $\rho = 2B_n/N(N-1) = \sum_{i,j} A_{i,j}/N(N-1)$, where $N(N-1)/2$ is the maximum number of edges for an N -site network. Note that $\rho \in [0, 1]$ and basically quantifies how sparse a network is. Figure 6 shows this measure for the three networks. They all yield $\rho \propto N^{-\alpha}$, with $\alpha = 1$, thus becoming increasingly sparse with N . In that regime the average degree tends to a constant, namely $\langle k \rangle = B_n/N_n = 1 - 1/N_n \rightarrow 1$ (0-AsN and 1-AsN) and $\langle k \rangle = 3 - 6/N_n \rightarrow 3$ (AN).

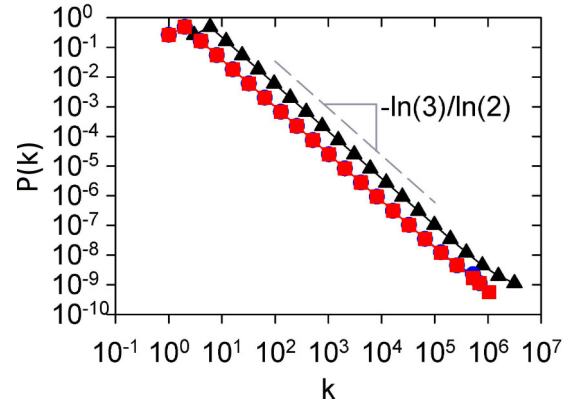


FIG. 5. Degree distribution $P(k)$ for the AN (black triangles), 0-AsN (blue circles), and 1-AsN (red squares). All of them display the scale-free property, $P(k) \propto k^{-\gamma}$, with $\gamma = \ln 3 / \ln 2$.

The AN is specially known for its small-world property. To account for this the average length of the shortest path is usually employed:

$$L = \frac{1}{N(N-1)} \sum_{i \neq j} d_{i,j}, \quad (2)$$

where $d_{i,j}$ is the length of the shortest path between nodes i and j . In Fig. 7 we evaluate it for both subnetworks and the AN, and note that $L \propto (\ln N)^\beta$, with $\beta = 3/4$ signaling the intermediate behavior between small- ($L \propto \ln N$) and ultrasmall-world [$L \propto \ln(\ln N)$] networks found in [4] for the AN. Now, the network diameter $d_n = L_{\max}$, that is the maximum shortest path among all the pairs of sites, is $d_n = 2n/3$ for the AN [18], considering $n \gg 1$ and $d_n = 2n + 1$ ($d_n = 2n$) for the 0-AsN (1-AsN). Hence, for large N we have that $L_{\max} \approx 2 \log(N)/(3 \log(3))$ in the AN and $L_{\max} \approx 2 \log(N)/\log(3)$ in both subnetworks.

One striking difference between the AN and the subnetworks comes from the local clustering coefficient C . It is known that a high value of C is another signature of the small-world property. However, while in the AN it tends to $C = 0.828$ for large N [4], the subnetworks yield $C = 0$. As

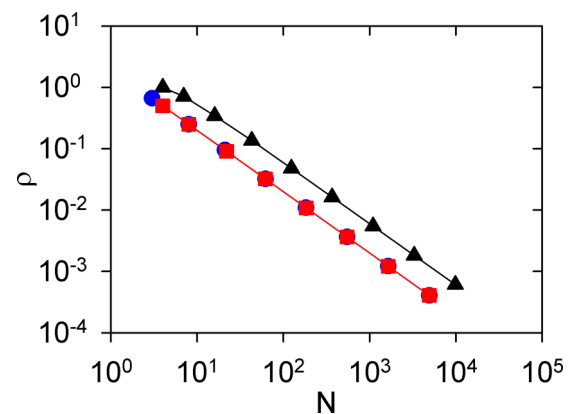


FIG. 6. Connectance $\rho = \sum_{i,j} A_{i,j}/N(N-1)$ vs network size N for the AN (black triangles), 0-AsN (blue circles), and 1-AsN (red squares). In each of these $\rho \propto N^{-1}$.

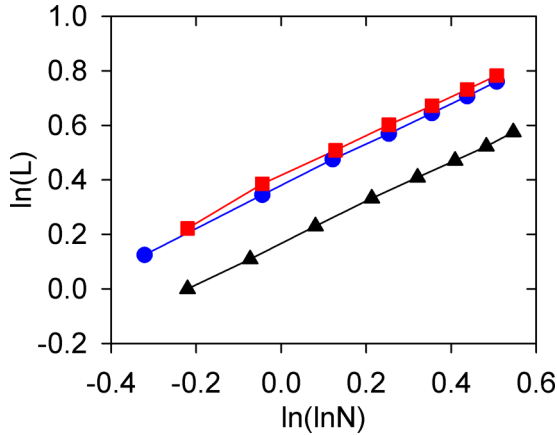


FIG. 7. Logarithm of average length of the shortest path versus $\ln(\ln N)$ for the AN (black triangles), 0-AsN (blue circles), and 1-AsN (red squares). Each gives $L \propto (\ln N)^\beta$, with $\beta = 3/4$.

mentioned before, they are tree-like structures and given C is proportional to the number of triangles in a network, one readily concludes that $C = 0$. Nevertheless, their small-world character is due to the presence of hubs (see Figs. 3 and 4).

We now move on to study some spectral properties of the adjacency matrix \mathbf{A} of each of the subnetworks. Its spectrum is equivalent to that of a tight-binding model defined on it, that is a Hamiltonian of the form $\mathbf{H} = J\mathbf{A}$, with $J \equiv 1$ being the hopping strength. As such, a lot can be inferred from the degree of localization of the single-particle states. Note that both subnetworks have undirected edges. That is to say, their adjacency matrices are symmetric and therefore have spectral decomposition. Both 0-AsN and 1-AsN networks have the bipartite property, meaning that the set of nodes in each of them is divided into two disjoint subsets (S_1 and S_2). As a consequence, the eigenvalue spectrum $\{\lambda_i\}$ is symmetric, $\lambda_{N+1-i} = -\lambda_i$ for all i . In Fig. 8 we show the density of states $DOS(\lambda) = \frac{1}{N} \sum_i \delta(\lambda - \lambda_i)$, δ being Dirac delta function, for the ninth generation. In both the 0-AsN and 1-AsN most of the

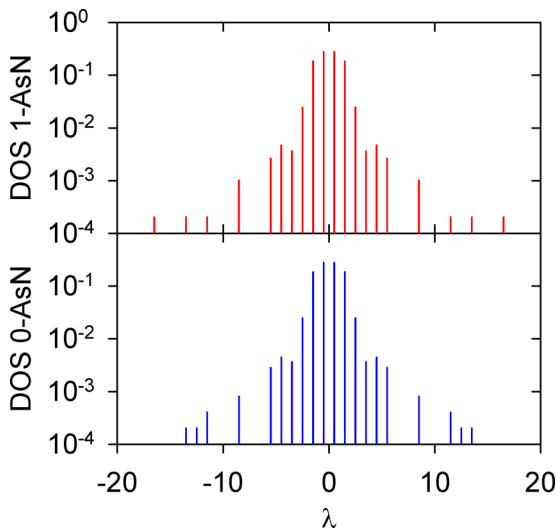


FIG. 8. Density of states of the adjacency matrix of the 0-AsN and 1-AsN for generation $n = 9$.

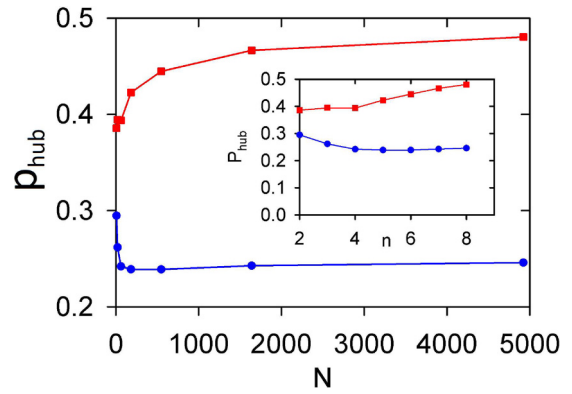


FIG. 9. Probability amplitude of the hub node p_{hub} vs N (and generation n ; see inset) considering the eigenvector having largest eigenvalue. The 0-AsN (1-AsN) is depicted by blue circles (red squares).

states populate the center of the band. One clear difference is that the 1-AsN is able to span more extreme modes. In the regular AN, modes lying far away from the center of the band carry a high degree of localization, mostly due to the nodes having highest number of connections [7,9]. To see how it goes for the subnetworks let us analyze the eigenvector with largest eigenvalue $|\lambda_{\text{max}}\rangle = [v_1, v_2, \dots, v_N]^T$, with $p_i = |v_i|^2$ being the probability amplitude for node i . Figure 9 shows such amplitude for the nodes having the maximum degree against size N . Note from Figs. 3 and 4 that the 0-AsN contains two equivalent hubs whereas the 1-AsN holds the hub of the original AN (cf. Fig. 2). We observe that p_{hub} converges to $1/4$ ($1/2$) as N grows on the 0-AsN (1-AsN).

Just like in the AN [7,9], here we find a high degree of localization in nodes having the highest number of connections. Thus, for large N we get a 50% chance to find the quantum particle at the hub nodes. Indeed, in [19] it was proved analytically that the probability of finding the particle in any of the sets S_1 and S_2 is equal for any bipartite lattice. As such, both subnetworks fulfill $\sum_{i \in S_1} p_i = \sum_{i \in S_2} p_i = 1/2$. Recall that the 0-AsN has two hubs, one at each S_1 and S_2 set of nodes. As these are equivalent, both hubs share nearly half of the total available probability amplitude. Now, the two sets are not equivalent in the 1-AsN. If we consider the subset to which the (single) hub belongs, it is observed that the eigenvector is almost fully localized at it and does not overlap with any node from the other subset, as expected.

IV. FINAL REMARKS

As seen above, the treelike subnetworks inherit many traits of the original AN, including its rich spectral structure with the onset of gaps and strong localization at the hubs. It is therefore expected that they also display a variety of transport regimes [8,9] and distinct condensed-matter properties in the light of a tight-binding approach [5,6,12]. The fact that connectivity of the nodes from younger generations diverges as N increases is associated with a power-law scaling of the energy gap between ground and first excited levels with N of the form $\Delta\lambda \propto N^\theta$ [20,21]. Then if we think, for instance, of noninteracting bosons hopping across such networks, at low

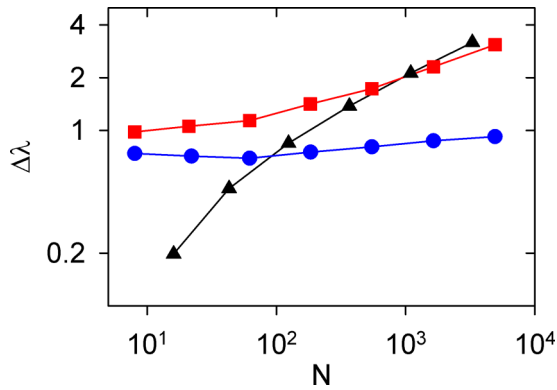


FIG. 10. Gap between the ground and first excited states $\Delta\lambda$ (in units of J) for the AN (black triangles), 0-AsN (blue circles), and 1-AsN (red squares).

temperatures the particles will be mostly concentrated in the sites from earlier generations, especially the hubs. In [6] a topology-induced Bose-Einstein condensation was addressed in the AN and the transition temperature was found to obey $T_c \propto N^{1/3}$, thus reflecting the scaling of the gap $\Delta\lambda$. In Fig. 10 we display the behavior of the gap against the system size N for the AN and its spawned subnetworks. For large N the former indeed exhibits $\theta = 1/3$, with the 0-AsN (1-AsN) rendering $\theta = 0.06$ (0.26). Note that the 1-AsN carries nearly the same scaling exponent as the AN and this is due to the presence of the original hub in it. It would thus be interesting to conduct further investigations regarding the degree of similarity between each of the subnetworks and the AN in that and other contexts.

We have obtained two subnetworks from the standard AN by assigning a bit to each one of the nodes and setting its growth to follow successive modulo 2 additions on a binary

TABLE I. Main properties of the Apollonian subnetworks in comparison with the original AN. $\langle k \rangle$ is the average degree, $C_{N \rightarrow \infty}$ is the clustering coefficient, d_n is the network diameter, α is related to the connectance $\rho \propto N^{-\alpha}$, β is the small-world exponent, γ is the degree distribution exponent, and θ comes from the power-law scaling for the gap between ground and first excited states, $\Delta\lambda \propto N^\theta$.

	AN	0-AsN	1-AsN
$\langle k \rangle$	$3 - \frac{6}{N_n}$	$1 - \frac{1}{N_n}$	$1 - \frac{1}{N_n}$
$C_{n \rightarrow \infty}$	0.828	0	0
d_n	x	$2n + 1$	$2n$
α	1.0	1.0	1.0
β	3/4	3/4	3/4
γ	$\ln(3/2)$	$\ln(3/2)$	$\ln(3/2)$
θ	0.34	0.06	0.26

version of it. Those novel structures happen to feature their own growth rules, developing a dendritic pattern. We found that both subnetworks share many characteristics with their original AN, including the small-world property. However, the clustering coefficient is zero due to the fact that no triangles can be formed among the nodes. Table I summarizes our main findings in comparison with the original AN.

They reveal that many emerging structures found in nature as well as in manufactured systems, such those that feature multi-branch tree growth, may share more similarities with the deterministic AN [4] than one would think.

ACKNOWLEDGMENT

We thank A. M. C. Souza for presenting us with the original idea and sharing key insights. This work was supported by CNPq.

[1] R. Albert and A.-L. Barabási, *Rev. Mod. Phys.* **74**, 47 (2002).
 [2] M. E. J. Newman, A.-L. Barabási, and D. J. Watts, *The Structure and Dynamics of Networks* (Princeton University Press, Princeton, NJ, 2006).
 [3] D. J. Watts and S. H. Strogatz, *Nature (London)* **393**, 440 (1998).
 [4] J. S. Andrade, H. J. Herrmann, R. F. S. Andrade, and L. R. da Silva, *Phys. Rev. Lett.* **94**, 018702 (2005).
 [5] A. M. C. Souza and H. J. Herrmann, *Phys. Rev. B* **75**, 054412 (2007).
 [6] I. N. de Oliveira, F. A. B. F. de Moura, M. L. Lyra, J. S. Andrade, Jr., and E. L. Albuquerque, *Phys. Rev. E* **81**, 030104(R) (2010).
 [7] A. L. Cardoso, R. F. S. Andrade, and A. M. C. Souza, *Phys. Rev. B* **78**, 214202 (2008).
 [8] X.-P. Xu, W. Li, and F. Liu, *Phys. Rev. E* **78**, 052103 (2008).
 [9] G. M. A. Almeida and A. M. C. Souza, *Phys. Rev. A* **87**, 033804 (2013).
 [10] L. de Arcangelis and H. J. Herrmann, *Front. Physiol.* **3**, 62 (2012).
 [11] R. F. S. Andrade and H. J. Herrmann, *Phys. Rev. E* **71**, 056131 (2005).
 [12] I. N. de Oliveira, F. A. B. F. de Moura, M. L. Lyra, J. S. Andrade, Jr., and E. L. Albuquerque, *Phys. Rev. E* **79**, 016104 (2009).
 [13] R. F. S. Andrade, J. S. Andrade, Jr., and H. J. Herrmann, *Phys. Rev. E* **79**, 036105 (2009).
 [14] B. Yang, P. Xie, and Z. Zhang, *Phys. Lett. A* **381**, 3773 (2017).
 [15] P. Xie, B. Yang, Z. Zhang, and R. F. S. Andrade, *Physica A* **502**, 40 (2018).
 [16] A.-L. Barabási and H. E. Stanley, *Fractal Concepts in Surface Growth* (Cambridge University Press, Cambridge, 1995).
 [17] K. Falconer, *Fractal Geometry: Mathematical Foundations and Applications* (John Wiley, Chichester, 1990).
 [18] Z. Zhang, F. Comellas, G. Fertin, and L. Rong, *J. Phys. A: Math. Gen.* **39**, 1811 (2006).
 [19] A. M. C. Souza, R. F. S. Andrade, N. A. M. Araújo, A. Vezzani, and H. J. Herrmann, *Phys. Rev. E* **95**, 042130 (2017).
 [20] N. Alon, *Combinatorica* **6**, 83 (1986).
 [21] K.-I. Goh, B. Kahng, and D. Kim, *Phys. Rev. E* **64**, 051903 (2001).